Journal of Solid State Chemistry **143,** 132–139 (1999)
Article ID jssc.1998.8127, available online at http://www.idealibrary.com on IDEAL®

Magnetic Structure and Spin Reorientation Transition in $ScMnO_3$

M. Bieringer and J. E. Greedan[1]

Brockhouse Institute for Materials Research and Department of Chemistry, McMaster University, Hamilton, ON L8S 4M1, Canada

Received August 27, 1998; in revised form November 17, 1998; accepted December 20, 1998

The magnetic structure of $ScMnO_3$ was investigated using polycrystalline samples. Bulk magnetic measurements were carried out revealing a Neel temperature of 130 K, followed by two maxima at 58 K and 40 K. The high-temperature data indicate strong antiferromagnetic coupling between Mn^{3+} ions in the form of a large, negative $\theta = -943(7)$ K. Powder neutron diffraction as a function of temperature disclosed magnetic long-range ordering below 130 K, where the chemical and magnetic unit cell have the same volume. A 120° magnetic structure was found consistent with the triangular Mn^{3+} sublattice and frustrated antiferromagnetic nearest neighbor coupling. The orientation of the magnetic spins is temperature dependent below 70 K. © 1999 Academic Press

***Key Words*: geometrical frustration; antiferromagnetism; spin reorientation.**

INTRODUCTION

Rare earth manganese oxides of composition $AMnO_3$ have been studied extensively. These oxides form an orthorhombic perovskite structure for large A, Pr^{3+}–Dy^{3+}, but hexagonal structures for smaller A, Ho^{3+}–Lu^{3+} (1). The hexagonal structure is described in $P6_3cm$ and is a distorted form of the $YAlO_3$ structure with A in sevenfold monocapped octahedral coordination and Mn in fivefold trigonal bipyramidal coordination. For the hexagonal structure a linear relationship exists between the rare earth cationic radii and the unit cell parameters a and c. To extend the series, $InMnO_3$ and $ScMnO_3$ are of interest as both In^{3+} and Sc^{3+} have smaller radii than Lu^{3+}. $InMnO_3$ has been found to have an anomalously long c-axis which has been rationalized in terms of the difference in electronic configurations between In^{3+} and the trivalent lanthanides. $ScMnO_3$ was first reported by Koehler *et al.* (2) but the structural analysis was not detailed. A later study by Norrestam (3) using single crystal data was not conclusive regarding the space group. The structure of $ScMnO_3$ was eventually established by Greedan *et al.* (4) in $P6_3cm$ and is thus isostructural with the remaining $AMnO_3$ phases.

[1]To whom correspondence should be addressed.

The magnetic structure of the A = Ho, Er, Tm, and Lu members of the series were determined by Koehler *et al.* (2) and a noncollinear 120° structure is found, consistent with the edge-shared triangular Mn^{3+} sublattice which is seen clearly in Fig. 1. The moments lie in the hexagonal plane. In $HoMnO_3$ an inplane spin reorientation occurs at temperatures below the Néel temperature but no such effect is seen for the other series members. The Néel temperature increases monotonically with decreasing c-axis length from $T_N = 76$ K for A = Ho to $T_N = 96$ K for A = Lu. From susceptibility and heat capacity measurements, Xu *et al.* determined a $T_N = 129$ K for $ScMnO_3$ (5). The magnetic structure of $InMnO_3$ is quite different from the remaining $AMnO_3$ phases as ordering of a long but finite range sets in below 120 K and there is clearly a c-axis doubling not found in the other series members (4).

As to-date, studies of $ScMnO_3$ have been sparse, this work reports magnetic susceptibility data over a wide temperature range, 5 to 600 K, on powder and single crystal samples and neutron diffraction studies of the magnetic structure.

EXPERIMENTAL

Preparation of $ScMnO_3$

Polycrystalline $ScMnO_3$ was prepared using Sc_2O_3 and Mn_2O_3 or Sc_2O_3 and MnO_2 which resulted in the same product. The well-homogenized mixture was pressed into pellets, which were reacted on a Pt-foil in an alumina boat for a total of 70 h at 1280^0C in air, which included several regrinding and refiring stages. The product formation was followed using a Guinier–Hägg camera. The dark gray product was covered with a greenish layer, which was removed. A small excess of approximately 4% Mn_3O_4 was detected. The preparation of single crystals can be found elsewhere (4).

Magnetic Measurements

Magnetic measurements were performed using a Quantum Design MPMS SQUID magnetometer in a temperature

0022-4596/99 $30.00
Copyright © 1999 by Academic Press
All rights of reproduction in any form reserved.

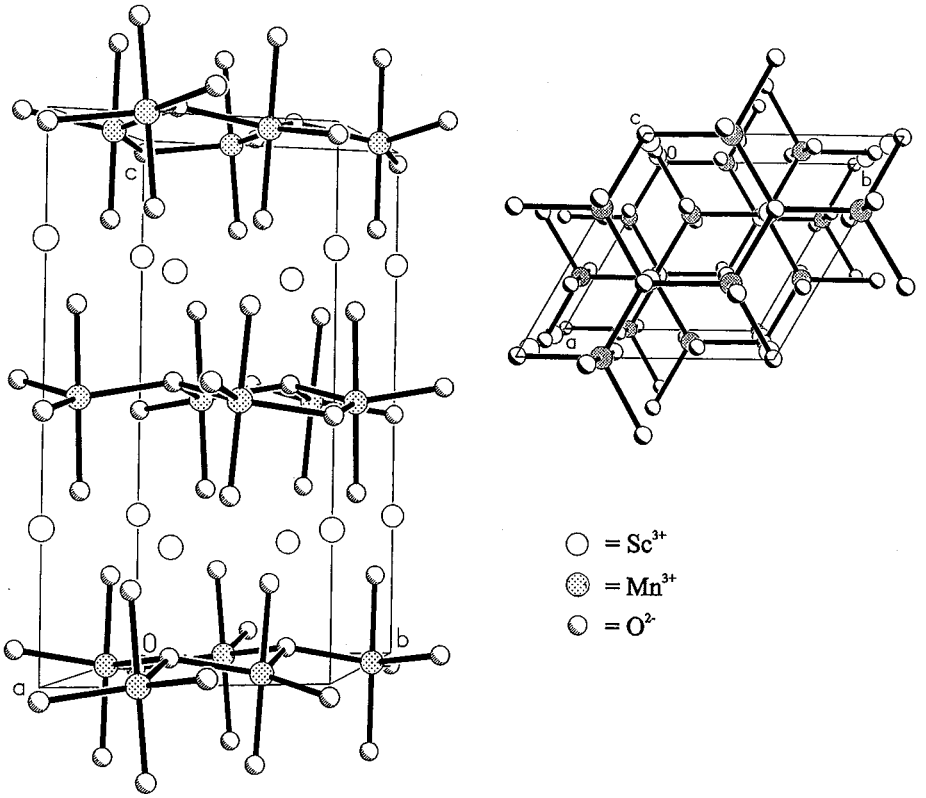

FIG. 1. Crystal structure of $ScMnO_3$.

range from 5 to 350 K and an applied magnetic field of 0.05 T. High-temperature measurements were carried out between 300 and 600 K using a furnace. Magnetic susceptibilities were measured using polycrystalline samples in order to obtain averaged data.

X-ray powder Diffraction

Powder diffraction data were obtained using a Guinier–Hägg camera having Cu$K\alpha_1$ radiation ($\lambda = 1.54056$ Å) and silicon as an internal standard.

The final polycrystalline product was investigated using a Nicolet I2 automated powder X-ray diffractometer having radiation Cu$K\alpha_{1,2}$ with $\lambda = 1.5418$ Å. The data were collected at room temperature over the diffraction angle range $10^0 \leq 2\theta \leq 90^\circ$; the step size was chosen to be $\Delta 2\theta = 0.03^\circ$. The collected data have been refined using the Rietveld refinement program Fullprof version 3.5. The single crystal X-ray diffraction data have already been published elsewhere (4).

Neutron Diffraction

All neutron powder diffraction experiments were carried out on the C2 diffractometer operated by the Neutron Program for Materials Research of the National Research Council of Canada at the Chalk River Nuclear Laboratory. The neutron wavelength was $\lambda = 1.32587$ Å.

The experiments were performed using an approximately 2 g sample in a vanadium can sealed under He gas with an indium wire gasket. Twenty-one data sets were collected between 10 and 130 K covering a 2θ-range from 10° to 90° (800 data points). The Rietveld refinement was performed using the program Fullprof version 3.5 (7). Three phases were included in the refinement, namely the chemical and magnetic structures of $ScMnO_3$ and the chemical structure of Mn_3O_4.

RESULTS AND DISCUSSION

Crystal Structure

The unit cell of $ScMnO_3$ contains six formula units and crystallizes in space group $P6_3cm$ (No. 185).

Figure 1 shows the unit cell. The stacking can be described as alternating Sc^{3+} layers and O–Mn–O layers separated by O^{2-} layers along the *c*-axis. With respect to the Mn^{3+} layers the stacking occurs in an $\cdots ABAB \cdots$ fashion, which is a rather rare stacking sequence for ternary hexagonal transition metal oxides.

Mn^{3+} is located in site 6*c* and forms a 2-dimensional net which is perfectly planar triangular. Two different sites are occupied by Sc^{3+}; Sc(1) is located in site 2*a* and Sc(2) in site

TABLE 1
Crystallographic Data for Polycrystalline $ScMnO_3$ from X-Ray Powder Diffraction Refinement

Crystal system	Hexagonal
Space group	$P6_3cm$
Unit cell dimensions (Å)	$a = 5.8364(2)$
	$c = 11.1812(5)$
Volume (Å^3)	329.84(2)
Z	6
Density (calc) (Mg/m^3)	4.490
Formula weight (g/mol)	147.90

4*b*. The Sc^{3+} ions form a net in the *a–b* plane which is slightly nonplanar.

The coordination of Mn^{3+} by O^{2-} gives rise to a distorted trigonal bipyramid, and these trigonal bipyramids are tilted with respect to the unit cell axis *c*. Sc^{3+} is sevenfold coordinated in both sites and forms monocapped octahedra when coordinated by O^{2-}.

The room-temperature powder neutron data were refined for two phases, namely $ScMnO_3$ and Mn_3O_4. Twenty-three parameters were refined including six background parameters, the cell constants and scale factors for both phases, the zero point as well as profile parameters, and nine atomic parameters for $ScMnO_3$. The amount of Mn_3O_4 present was refined to be 5.4(6) wt%. The atomic parameters for $ScMnO_3$ are given in Table 2, the unit cell constants can be obtained from Table 1. The final agreement factors are $R_p = 4.53$, $R_{wp} = 6.01$, and $\chi^2 = 5.20$. The structure of $ScMnO_3$ deduced using single crystal data (4) and the polycrystalline sample, using X-ray and neutron diffraction data which are published in this work, are in agreement. Thus this serves as support for the correctness of the assumed model for the powder sample.

Magnetic Susceptibilities

Figure 2 shows the magnetic susceptibility for polycrystalline $ScMnO_3$ using a field strength of 0.05 T. Three

TABLE 2
Atomic Coordinates and Equivalent Isotropic Displacement Parameters for Polycrystalline $ScMnO_3$ at Room Temperature from Neutron Powder Data Refinement

	x	*y*	*z*	*U*(eq) (Å^2)
Sc(1)	0	0	0.2793(12)	0.39(4)
Sc(2)	1/3	2/3	0.2335(10)	0.39(4)
Mn	0.3333(2)	0	0	0.50
O(1)	0.3995(15)	0	0.1645(13)	0.11(6)
O(2)	0.6381(16)	0	0.3307(14)	0.11(6)
O(3)	0	0	0.4788(15)	0.11(6)
O(4)	1/3	2/3	0.0248	0.11(6)

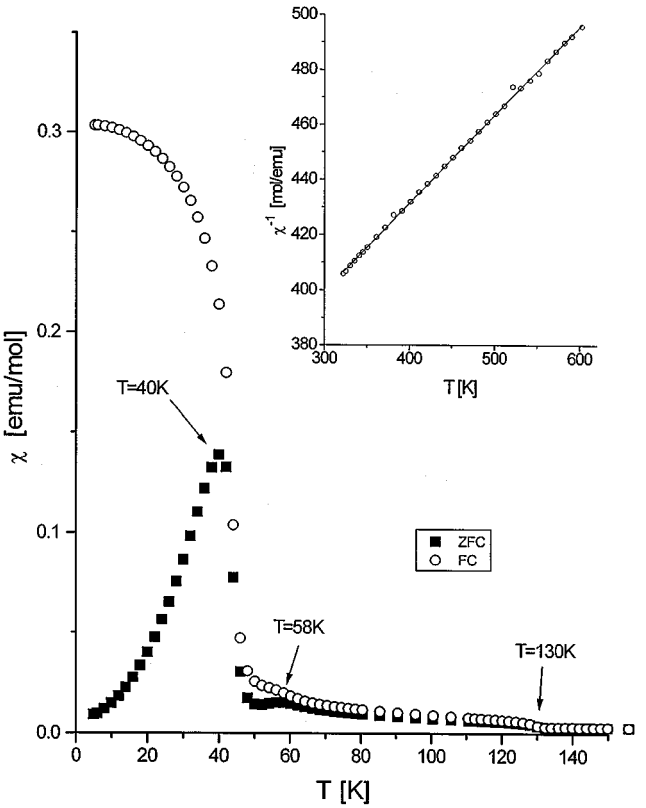

FIG. 2. Magnetic susceptibility for polycrystalline $ScMnO_3$ using a magnetic field of 0.05 T, solid squares, zero field cooling data; open circles, field cooling data. The inset shows the Curie–Weiss fit for the temperature range from 320 to 600 K.

significant features are present, namely an inflection point at 130 K, a broad maximum at 58 K, and a maximum at 40 K.

The Néel temperature is 130 K, below which magnetic long range ordering occurs. Note the FC-ZFC divergence below 130 K which indicates the presence of weak ferromagnetism due to sublattice canting. The broad maximum at 58 K is due to spin reorientation. The transition at 40 K is due to spin canting. It should be mentioned that this feature is not caused by the Mn_3O_4 impurity. This was evaluated from a study carried out earlier on different samples which showed the presence of a larger Sc_2O_3 impurity but no Mn_3O_4 impurity. All samples showed a maximum at 40 K. Furthermore, magnetic susceptibility data acquired using single crystals showed a maximum at 40 K as well. The high-temperature data, collected in a separate experiment, are shown as an inset in Fig. 2. The Curie–Weiss law was found for the temperature range 320–600 K, a temperature independent term being of no significance,

$$\chi = \frac{C}{T - \theta_c}, \qquad [1]$$

where χ is the molar magnetic susceptibility, C is the Curie constant, and θ_c is the Weiss temperature.

Accounting for 4 wt% of Mn_3O_4, the Curie constant for $ScMnO_3$ was found to be 2.85(3) emu K/mol, giving an effective magnetic moment of 4.78(4) μ_B which is close to the theoretical spin only value of 4.9 μ_B for Mn^{3+}. The Weiss temperature is $\theta_c = -943(7)$ K indicating strong antiferromagnetic coupling.

Xu *et al.* published a Néel temperature of 129 K determined from magnetic data and heat capacities (5) and is therefore close to our value. These authors did not measure the temperature range below 77 K where additional transitions are found.

Magnetic Structure

The magnetic structure of $ScMnO_3$ is expected to reflect the geometric frustration inherent in the triangular lattice with strong antiferromagnetic exchange. This situation is shown in Fig. 3.

Neutron diffraction experiments have been employed in order to determine the magnetic structure of $ScMnO_3$. Data were collected for 21 temperatures between 10 and 130 K. Figure 4 shows the low angle region of the powder neutron diffractograms obtained at several temperatures emphasizing the changing intensities of the most prominent magnetic Bragg reflections and finally the disappearance of the magnetic Bragg peaks at 130 K. The diffractograms below 130 K show additional peaks, which are due to magnetic long-range ordering. Upon lowering the temperature, the intensity of the $(101)_{mag}$ peak increases until a temperature of 70 K is reached; below 70 K the intensity decreases again and remains constant below 40 K. However, the $(100)_{mag}$ peak appears below 70 K and its intensity increases until a temperature of 40 K is reached. Between 40 and 10 K the intensity of the $(100)_{mag}$ reflection does not change significantly. All magnetic peaks can be indexed on the chemical unit cell. Therefore, the propagation vector is $\mathbf{q} = [000]$.

Below 45 K the $(100)_{mag}$ reflection shows a shoulder on the high-angle side, which is due to the strongest magnetic reflection of Mn_3O_4, which is present as a small impurity phase. The disappearance of this reflection above 40 K is in agreement with the ordering temperature of 42.5 K for Mn_3O_4 (6). The presence of the shoulder at low-temperature complicates the refinement of the magnetic structure which will be discussed in the next paragraph.

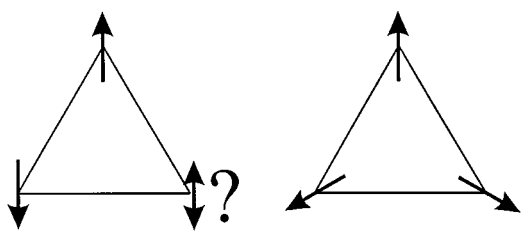

FIG. 3. Triangular arrangement of magnetic moments and the impossibility of satisfying all antiparallel alignments simultaneously. Right-hand side 120° structure.

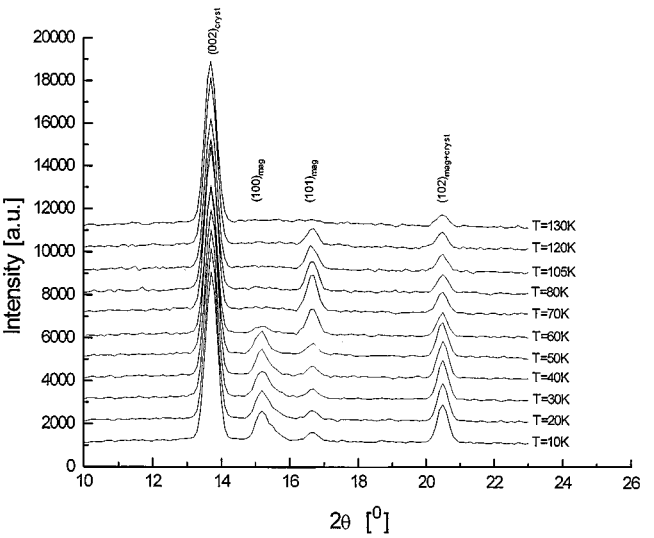

FIG. 4. Neutron powder diffraction patterns for $ScMnO_3$ at different temperatures, showing magnetic long rang order at low temperatures, $\lambda = 1.32587$ Å.

The varying intensity ratio of the $(100)_{mag}$ peak and the $(101)_{mag}$ reflection is due to spin reorientation in the **a**–**b** plane. Close to the Neel temperature a broad background can be seen.

Magnetic Short-Range Order

To estimate the correlation length associated with two-dimensional magnetic short-range order the neutron powder data were fitted to a Warren lineshape (8),

$$P_{2\theta} = Km \frac{F_{hk}^2(1 + \cos^2 2\theta)}{2(\sin\theta)^{3/2}} \frac{(L)^{1/2}}{\pi\lambda} F(a), \qquad [2]$$

where $a = (2\sqrt{\pi}L/\lambda)(\sin\theta - \sin\theta_0)$, K is a constant, m is the multiplicity, F_{hk} is the two-dimensional structure factor, λ is the wavelength, L is a two-dimensional correlation length, and θ_0 is the peak position. The function $F(a)$ is tabulated.

The results are shown in Fig. 5. The strongly overlapping $(002)_{cryst}$ was modeled using a gaussian lineshape. From the 130 K data set only the $(102)_{cryst}$ peak was excluded. Whereas, for lower temperatures the $(101)_{mag}$ reflection was excluded as well. Below 80 K too many peaks are present and no fit using the Warren function was carried out. A nearly temperature-independent correlation length of 13(2) Å for the temperature range 80–130 K was found.

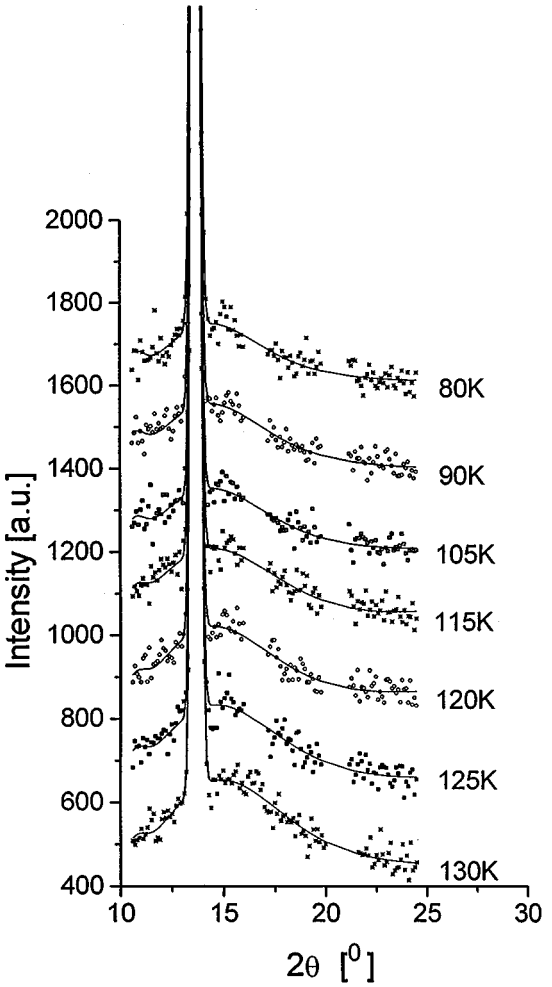

FIG. 5. Powder neutron diffraction data. Two-dimensional magnetic short-range order. The symbols are experimental data and the solid lines represent fits to a Warren line shape.

Refinement of the Magnetic Structure

All neutron diffraction refinements were done for three phases, namely the crystallographic structure for $ScMnO_3$, the magnetic structure for $ScMnO_3$, and Mn_3O_4 as a minor impurity phase. When refining the neutron powder diffraction data sets for various temperatures, 15 parameters were refined including the unit cell parameters, the zero point, the scale factors, the magnetic moments, and six background parameters.

The data were collected over a 2θ-range from 10^0 to 90^0. The orientation of the magnetic moments is strongly correlated to the intensity ratio of the $(100)_{mag}$ and the $(101)_{mag}$ reflections as was shown with neutron powder pattern simulations. Due to the presence of Mn_3O_4 the $(100)_{mag}$ peak is broadened at low temperature. Refinements were carried out using different strategies. In one case the refinement was carried out at 70 K and for all remaining data sets the peak shape parameters were held constant. During an alternative refinement procedure the $(100)_{mag}$ peak was excluded from the refinements. Between 10 and 70 K the same results were found for both procedures, but at higher temperatures the orientations for the magnetic moments differed such that the first procedure resulted in smaller angles, ϕ. This is caused by the broad background underneath the $(100)_{mag}$ and $(101)_{mag}$ peak which could not be modeled properly. This problem is illustrated in Fig. 6 where the calculated profile includes a small peak at the $(100)_{mag}$ position when none is present in the data. For the above-mentioned reasons the $(100)_{mag}$ peak was excluded from the Rietveld refinements. Below 35 K the region $23^0 < 2\theta < 24^0$ is excluded from the refinements, because of the presence of a magnetic peak due to Mn_3O_4 which is negligible above 30 K.

Initially, a 120° spin arrangement was assumed with the moments lying in the *a–b* plane, using space group *P*1 and a 120° rotation matrix. Figure 7 shows the initial model for the magnetic moments and the definition of the spin orientation ϕ. Powder neutron diffraction patterns of the magnetic phase were simulated assuming out-of-plane spin canting angles of 5° and 10°; the resulting patterns are too

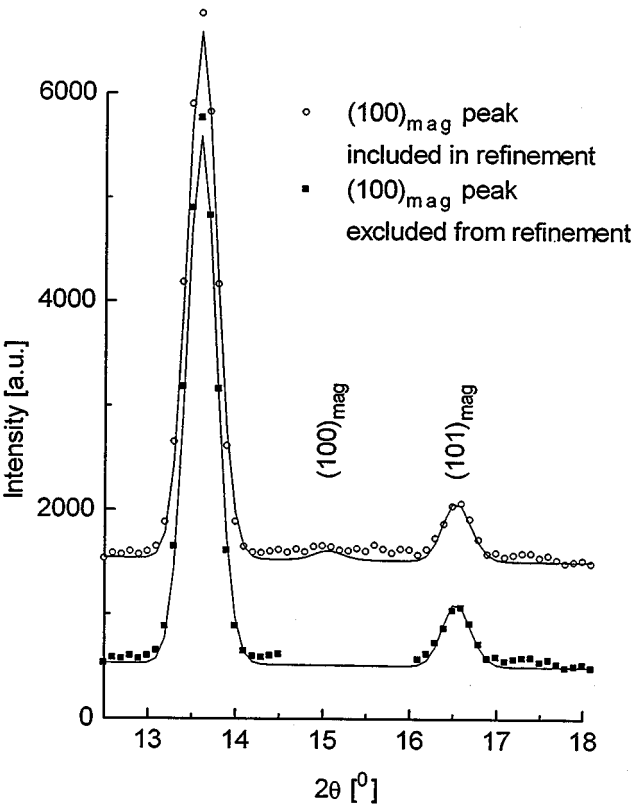

FIG. 6. Neutron powder diffraction patterns for $ScMnO_3$ at 120 K. Illustration of incorrect fitting of $(100)_{mag}$ peak as a consequence of the broad background present.

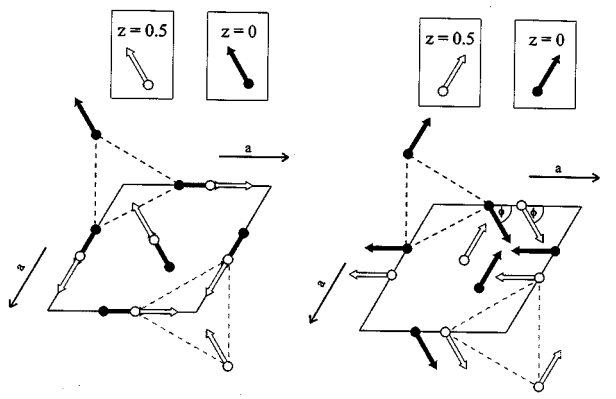

FIG. 7. Description of the magnetic structure of $ScMnO_3$ at two different temperatures; (right) low-temperature form and (left) high-temperature form. The 120° constraint is retained after reorientation of the magnetic moments in the basal plane. Only the Mn^{3+} positions are shown.

similar to the noncanted case to be distinguished by powder neutron diffraction techniques. Nonetheless, magnetic susceptibility data indicate weak ferromagnetism and support the presence of spin canting. Consequently, the neutron powder refinements were carried out assuming no canting of the spins.

For several temperatures the refined powder neutron diffraction data are shown in Fig. 8, and Table 3 shows the results for all refinements. The results for the orientations and magnitudes of the magnetic moments in $ScMnO_3$ are shown in Fig. 9. At 10 K the magnetic moments are almost aligned with the a-axis, i.e., $\phi = 15(3)^\circ$, at 40 K the spins start to reorient simultaneously in the a–b plane. At 70 K the reorientation reaches an angle of $\phi = 80(9)^\circ$, and therefore the spins are oriented almost perpendicularly with respect to the low-temperature case. The reorientation process occurs between 50 and 70 K, which is in agreement with the broad feature at 58 K for the magnetic susceptibility. The magnitude of the magnetic moment at 10 K is 3.40(7) μ_B and decreases rapidly above 90 K. Upon warming the sample, the unit cell parameter a increases, whereas the c-axis remains constant between 10 and 130 K (Fig. 10). The crystallographic structure of $ScMnO_3$ does not change

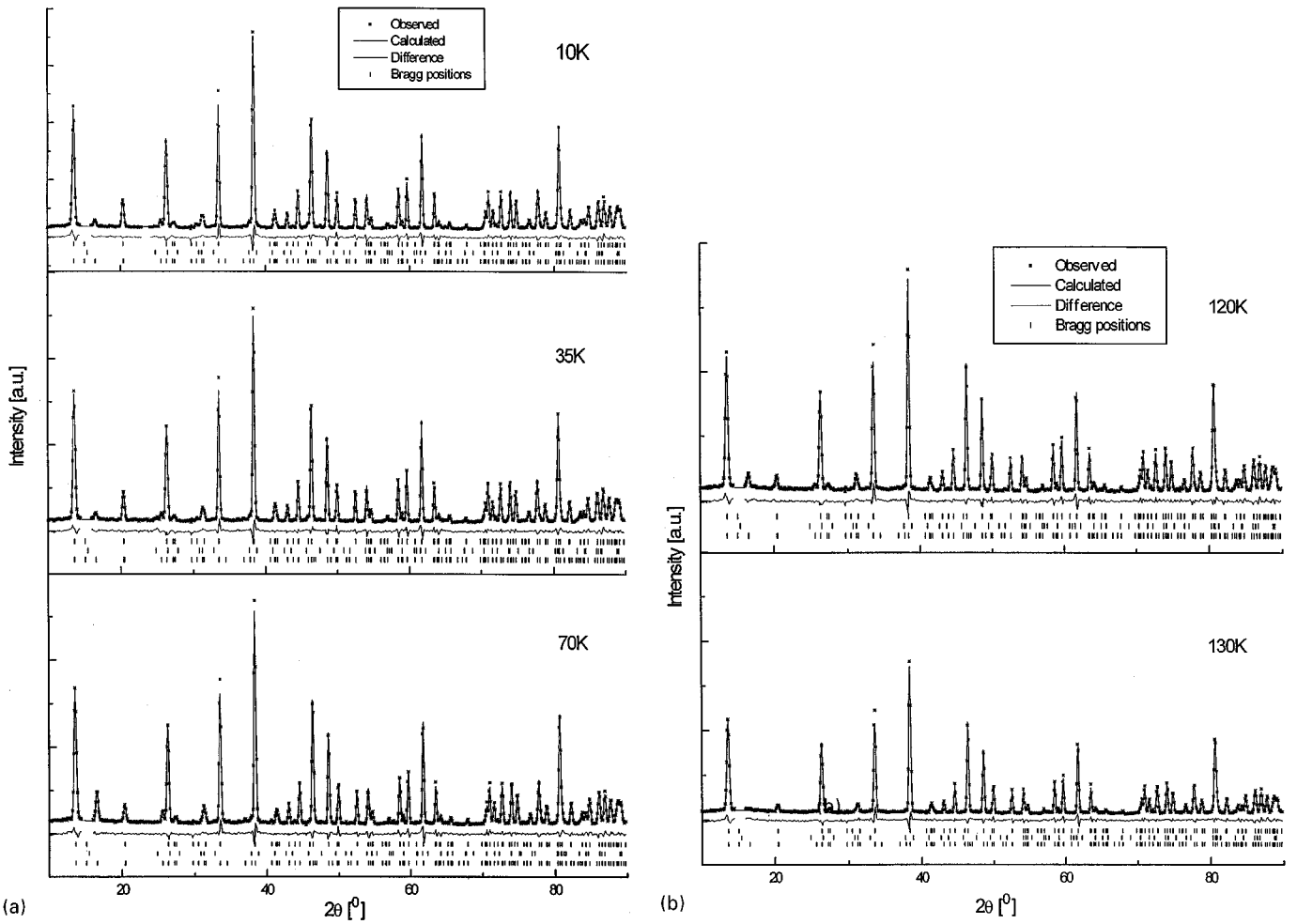

FIG. 8. Refined neutron powder diffraction patterns for (a) $T = 10$, 35 and 70 K and (b) $T = 120$ and 130 K. For all graphs the tick marks at the top refer to the crystallographic structure of $ScMnO_3$, in the middle to Mn_3O_4, and at the bottom to the magnetic structure of $ScMnO_3$.

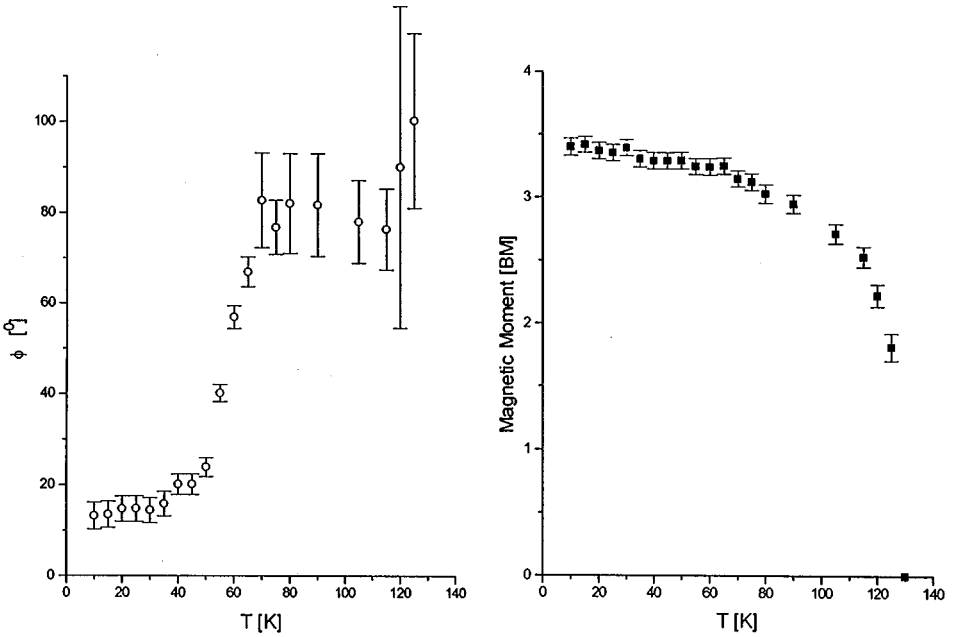

FIG. 9. The left figure shows the reorientation of the magnetic moments of Mn^{3+} in $ScMnO_3$ in the basal plane as a function of the temperature. The right figure shows the temperature dependence of the magnitude of the magnetic moment.

as a function of temperature as confirmed by carrying out full refinements at various temperatures.

CONCLUSIONS

Magnetic measurements carried out on $ScMnO_3$ over a wide temperature range, 5–600 K, show the presence of strong antiferromagnetic exchange, $\theta_c = -943(7)$ K, and three transitions, one at 130 K, a second, broad transition at 58 K, and a maximum at 40 K. Neutron diffraction experiments confirm that the 130 K transition represents the Néel temperature below which a 120° magnetic structure is found. This result is consistent with previous work on isostructural $LnMnO_3$ phases, Ln = Ho–Lu. The 120° structure arises due to the frustration inherent in the layered triangular Mn^{3+} sublattice and the very strong antiferromagnetic exchange already noted. The transition at 58 K is revealed by neutron diffraction to involve a spin reorientation of the moments within the a–b plane. At 10 K the Mn^{3+} spins are almost parallel to the a–a crystallographic axes but at 50 K they begin to reorient to an angle of 80° with respect to the a-axes which is complete at 70 K. This is similar to the behavior of $HoMnO_3$. Koehler *et al.* (2) reported a 120° structure for the magnetic moments in $ScMnO_3$, and an angle $\phi = 24°$ at 4.2 K, however, no temperature dependence of ϕ has been reported since.

The two-dimensional magnetic short-range order between 80 and 130 K can be described with a nearly temperature-independent correlation length of 13(2) Å.

The origin of the weak ferromagnetism and the maximum at 40 K in the ZFC magnetic susceptibility data mentioned earlier could be due to out-of-plane spin canting

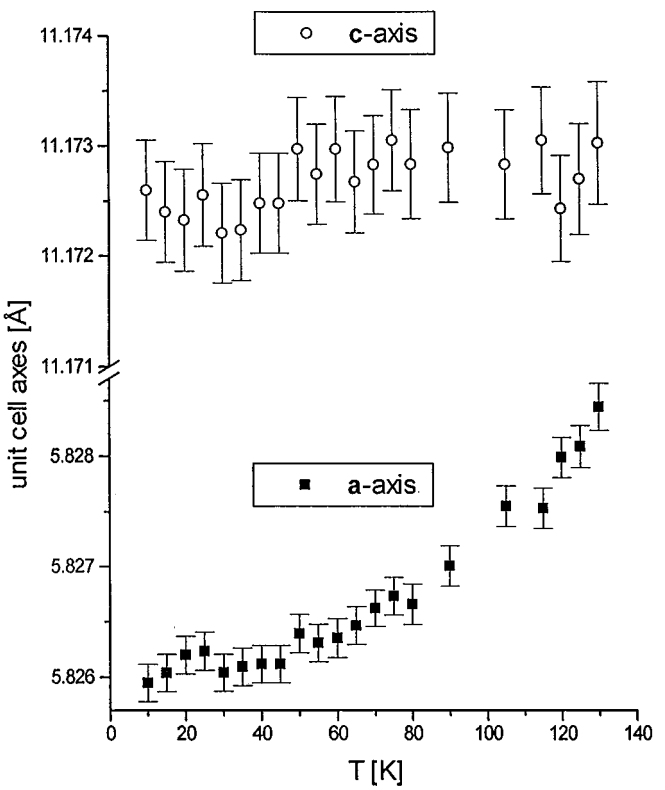

FIG. 10. Unit cell axes lengths for $ScMnO_3$ as a function of temperature.

TABLE 3
Three Phase Neutron Powder Diffraction Refinement for $ScMnO_3$ at Low Temperatures

T [K]	M [μ_B]	ϕ [°]	Magnetic-R^a	$R_p{}^b$	$R_{wp}{}^c$
10	3.40(7)	12(3)	12.8	5.16	6.67
15	3.40(7)	13(3)	13.3	5.32	6.71
20	3.36(7)	14(3)	11.2	5.23	6.76
25	3.34(7)	14(3)	13.0	5.26	6.78
30	3.39(7)	14(3)	12.3	5.20	6.64
35	3.28(7)	15(3)	13.7	5.21	6.65
40	3.29(7)	20(2)	12.6	5.20	6.63
45	3.29(7)	20(2)	12.6	5.20	6.63
50	3.27(7)	23(2)	13.7	5.43	6.90
55	3.23(7)	40(2)	11.9	5.28	6.67
60	3.23(7)	57(3)	12.8	5.42	6.95
65	3.23(7)	67(4)	11.7	5.24	6.75
70	3.14(7)	82(9)	11.2	5.00	6.44
75	3.11(7)	77(6)	13.1	5.22	6.60
80	3.01(8)	82(12)	12.4	5.66	7.14
90	2.93(8)	82(13)	16.0	5.55	7.12
105	2.69(8)	78(10)	13.6	5.55	7.08
115	2.51(9)	76(10)	18.9	5.55	6.97
120	2.20(10)	92(37)	19.5	5.51	7.00
125	1.81(12)	100(19)	30.9	5.66	7.17
130				6.07	7.59

$$^a\text{Magnetic} - R = 100\frac{\sum_k |I_{Ok} - I_{Ck}|}{\sum_k |I_{Ok}|}.$$

$$^bR_p = 100\frac{\sum_i |y_i - y_{ic}|}{\sum_i |y_i|}.$$

$$^cR_{wp} = 100\sqrt{\frac{\sum_i w_i[y_i - y_{ic}]^2}{\sum_i w_i y_i^2}}.$$

and was predicted by Kawamura for a layered triangular lattice (9).

A more detailed study would require large single crystals in order to perform neutron diffraction experiments and to investigate possible spin canting in $ScMnO_3$. Unfortunately, the crystal growth showed only a very slow growing rate along the c-direction, resulting in extremely thin crystals (5 μm). Slower cooling during the crystal growth resulted only in crystals with larger dimensions in the a–b plane. Therefore, the spin canting problem cannot be solved in the near future.

ACKNOWLEDGMENTS

We thank N. P. Raju for assistance with the SQUID magnetometer and H. Dabkowska for helpful discussions. M. Bieringer is grateful for financial support from the "Deutscher Akademischer Austauschdienst". J. E. Greedan acknowledges support from the Natural Sciences and Engineering Research Council of Canada.

REFERENCES

1. H. L. Yakel, W. C. Koehler, E. F. Bertaut, and E. F. Forrat, *Acta. Crystallogr.* **16**, 957–962 (1963).
2. W. C. Koehler, H. L. Yakel, E. O. Wollan, and J. W. Cable, *Phys. Lett.* **9**(2), 93–95 (1964).
3. Rolf Norrestam, *Acta Chem. Scand.* **19**, 1009–1010 (1965).
4. J. E. Greedan, M. Bieringer, J. F. Britten, D. M. Giaquinta, and H.-C. zur Loye, *J. Solid State Chem.* **116**, 118–130 (1995).
5. H. W. Xu, J. Iwasaki, T. Shimizu, H. Satoh, and N. Kamegashira, *J. Alloys Compounds* **221**, 274–279 (1995).
6. B. Boucher, R. Buhl, and M. Perrin, *J. Phys. Chem. Solids*, **32**, 2429–2437 (1971).
7. Juan Rodriguez-Carvajal, "Fullprof Manual version 3.5."
8. B.E. Warren, *Phys. Rev.* **59**, 693 (1941).
9. Hikaru Kawamura, *J. Phys. Soc. Jpn.* **54**(9), 3220–3223 (1985).